Indian J. Phys. **76B** (4), 371–378 (2002)

I J P B
— an international journal

New insights into small-angle electron scattering : guiding measurements

A Z Msezane and Z Felfli
Department of Physics and Center for Theoretical Studies of Physical Systems, Clark Atlanta University, Atlanta, GA 30314, USA
E-mail : amsezane@ctsps.cau.edu

Abstract : Firstly, we demonstrate that in an appropriate representation the apparent generalized oscillator strength (AGOS) manifests its general properties and that the zero scattering angle curve connects continuously the threshold energy $E = \omega$ and the high energy $E = \infty$, corresponding to the optical oscillator strength, without traversing the nonphysical region. Secondly, the recent generalized Lassettre expansion (GLE) [*Phys. Rev Lett.* **81** 961 (1998)] with only a single moving Regge pole is employed to establish the applicability of the Lassettre limit theorem regardless of the electron impact energy and to generate the associated normalization curve for the measured relative electron differential cross sections (DCS's). At forward scattering the GLE yields the unique and long-sought-after normalization curve to the optical oscillator strength of the measured relative DCS's through the AGOS. Optically allowed transitions in H, He and Xe are used to illustrate the normalization curve.

Keywords : Electron, scattering, oscillator, regge pole.

PACS Nos. : 34.80.Dp, 31.50.Df, 32.70.Cs, 34.10.+x

1. Introduction

For optically allowed transitions in atoms, ions and molecules, the major contribution to the integral scattering cross sections (ICS's) is considerably larger from the small angular region, particularly when the impact energy is large. However, in this angular region the measured electron DCS's are generally riddled with uncertainties due mainly to the difficulties in carrying out these measurements. The difficulties of measuring reliably the electron DCS's at the small scattering angles, including zero, well documented in the literature, are still clearly manifest even in the most recent measurements for H [1] and Li [2]. For the former, measurements were obtained down to only 7° at all the impact energies considered, while for the latter, data were obtained down to 6° at 21.8 eV. Similarly, the DCS's for Mg II, Zn II and Cd II were measured down to only 4°, 6° and 4°, respectively at 50 eV [3]. For molecular transitions the problem is exemplified by the vibronic excitation bands ($v = 1-4$) of the $b\ ^1\Pi_u$ electronic state of N_2 [4]. Additionally, DCS measurements at the least physically attainable scattering angle, zero, are obtained at values of the momentum transfer squared, $K^2 > 0$ regardless of impact energy, E. Hence, the behavior of the DCS in the non-physical region, finite E, defined by the region between the values of K^2 at $\theta = 0°$ and $K^2 = 0$, down to $K^2 = 0$ can not be achieved by experiment. Thus this behavior must be studied through theoretical representations.

The generalized oscillator strength (GOS) concept introduced by Bethe [5] manifests directly the atomic wave functions and the dynamics of atomic electrons. Important information about both the electron DCS's and ICS's can be obtained by investigating the behavior of the GOS as $K^2 \to 0$ [6], since the GOS converges to the optical oscillator strength (OOS) for $K^2 \ll 1$. Lassettre *et al* [7] established that this must be valid regardless of E, *viz.* whether the first Born approximation is applicable or not. One of the major problems encountered in extrapolating the measured GOS to the OOS, employing the standard Lassettre series [8], apart from the problem of convergence, has been that the non-physical region of the GOS becomes extensive as E decreases toward threshold, thereby making the extrapolation difficult and unreliable [9]. To remedy some of the problems, the Regge pole representation of the electron DCS was introduced [10].

The approach analytically continues the measured data from the larger angular region, where they are generally measured more reliably, through to zero scattering angles, where measurements are difficult to obtain.

Problems of determining absolute values of the measured electron DCS's using a GOS technique and contributions to the ICS's from the small angular regime have been discussed by Ismail and Teubner [11], who measured the DCS's for excitation of the resonance transition in Cu down to $\theta = 2°$ at all their impact energies. They also demonstrated that at 20 eV and 100 eV 84% and 99%, respectively of the contributions to the ICS's come from the approximate angular range $0 \le \theta < 15°$. This conclusion is consistent with the results found by Chen and Msezane [12] for optically allowed transitions in Xe and Na. Also, the contribution from the angular regime not covered by the measurement ($0 \le \theta < 6°$) to the ICS's in the electron excitation of the states $6s[3/2]_{1,2}$ of Xe was found [9] to be between 1% and 70% for E values between 15 eV and 100 eV, respectively.

Above we have demonstrated sufficiently that many measurements of the electron DCS's for optically allowed transitions in atoms obtain data only down to some small angle, θ_s near $\theta = 0°$ and almost never at $\theta = 0°$. (We note that the same applies to molecular transitions. The case of ionic transitions is even worse; there are very few measurements of DCS's for them because of severe technical difficulties). However, these transitions receive the major contribution to the ICS's mainly from the small angular range, particularly at high energies.

In this paper we first use the recently developed methods [10,13,14] to demonstrate the applicability of the Lassettre limit theorem over the entire electron impact energy, *viz.* from threshold, $E = \omega$ to the optical oscillator strength (OOS), $E = \infty$. Then, we show that at forward scattering the GLE represents the unique long-sought-after normalization curve to the OOS for the measured relative electron DCS's.

2. Theory

2.1. The momentum dispersion method (MDM) :

The DCS and the GOS for atomic or molecular excitation by a fast electron are related through (atomic units are used throughout) [5,15]

$$f(E,K^2) = \frac{\omega}{2}\frac{k_i}{k_f}K^2\left(\frac{d\sigma}{d\Omega}\right), \tag{1}$$

where

$$K^2 = 2E\left[2 - \frac{\omega}{E} - 2\sqrt{1-\frac{\omega}{E}}\cos\theta\right], \tag{2}$$

ω, k_i and k_f are respectively, the excitation energy, the electron momenta before and after collision, K and θ are the momentum transfer and scattering angle, and E is the impact energy.

We note that although eq. (1) is obtained within the applicability of the FBA, an apparent generalized oscillator strength (AGOS) can be defined so that the energy dependent eq. (1) is also applicable when the measured or calculated DCS's are used [15]. The limit of the AGOS as $K^2 \to 0$ (commonly known as the Lassettre limit theorem) is

$$f^0 = \lim_{K^2 \to 0} f(E,K^2). \tag{3}$$

Ester and Kessler [9] have found that for $E < 40$ eV their measured absolute data for the electron excitation of Xe to the states $6s[3/2]_{1,2}$ could not be extrapolated to the Lassettre limit, *viz.* the OOS, using the Lassettre formula [7,8] Also, the problem associated with the normalization of the measured relative electron DCS's through the standard Lassettre expansion, particularly when using relatively small impact energies, has been discussed. Haffad *et al* [10] discovered that the expansion coefficients in the Lassettre expansion increased dramatically with each new term, thereby limiting the utility of the expansion to only the generally more inaccurately measured small angular data. To circumvent this problem Haffad *et al* have used a dispersion relation representation of the DCS's for dipole allowed transitions at small K^2 values. The Regge pole representation of the electron DCS's transforms eq. (1) to (10)

$$F(x^2) = \frac{1}{(1+x^2)^6}\left[R + 2r\cos\left(\varepsilon\log(1+\xi x^2) - \phi\right)\right], \tag{4}$$

where $x = K/Y$ with $Y = \sqrt{2I} + \sqrt{2(I-\omega)}$, I and ω being the ionization and excitation energies, respectively. The quantities R, r, ε and ϕ are yet to be determined. Eq. (4) is mapped through

$$z = \log(1+x^2) \quad \text{and} \quad F^M(z) = (1+x^2)^6 F(x^2), \tag{5}$$

which reduce eq. (4) to

$$F^M(z) = a_0 + a_1\cos\varepsilon z + b_1\sin\varepsilon z, \tag{6}$$

where $a_0 = R$, $a_1 = 2r\cos\phi$, and $b_1 = 2r\sin\phi$. In the new system of variables the AGOS is expanded in a Fourier series of which we have retained only the first terms determined from eq. (6) and $\log(1+x^2)$ is a natural variable. The OOS is then

$$f^0 = a_0 + a_1. \tag{7}$$

The parameters a_0, a_1, b_1 and ε are determined by minimizing $F^M(z)$ through the functional

$$\mathcal{F} = \sum_{i=1}^{N}\left[\frac{F_i^{\exp} - F^M(z_i)}{\Delta F_i^{\exp}}\right]^2, \tag{8}$$

where N is the number of experimental data points, z_i, F_i^M and ΔF_i^M are the mapped *experimental* values through the mapping eq. (5) of the i-th point position, the AGOS value and error in the AGOS, respectively. The dependence of F^M on z is irrelevant to the outcome of the parameters. This is a very

fine and desirable feature of the method because the investigations of F^M as a function of a new variable will not result in a new derivation, but only in a modification in the definition of both F^M and z. We stress that the OOS's are automatically extracted with the constants, a_0, a_1, b_1 and ε in the method. The correct OOS's therefore provide self-consistency checks of the measurements.

Eq. (6) represents the expression for the MDM. In an appropriate representation the AGOS varies linearly with K^2 so that the difficult to measure smaller angular data can be obtained readily through analytical continuation. The MDM has been used extensively to obtain smaller angular data from larger angular measurements and to calculate ICS's for transitions in Xe and N_2 [16]. Also, with some modification it has been used successfully to analyze optically forbidden transitions in atoms and molecules [17].

2.2 Forward scattering function (FSF) :

Avdonina *et al* [13] have introduced the dimensionless variables

$$y = \cos(\theta),\ u = \frac{K^2}{2\omega} \text{ and } t = \frac{\omega}{E}, \tag{9}$$

to transform K^2 to

$$ut = 2 - t - 2\sqrt{1-ty}, \tag{10}$$

where $0 \le t \le 1$, $u \ge 0$ and y is without restriction. The physical region corresponds to $|y| \le 1$ while $|y| > 1$ defines the nonphysical region. At fixed y the energy parameter t has two values. When $u \sim 1$, they are

$$t_1 \sim 4u/(1+u)^2 \quad \text{and} \quad t_2 = 2\sin^2\theta/(1+u)^2. \tag{11}$$

Notably, t_1 is independent of θ and corresponds to the forward scattering ($\theta = 0°$) of the AGOS [13], see Figure 1.

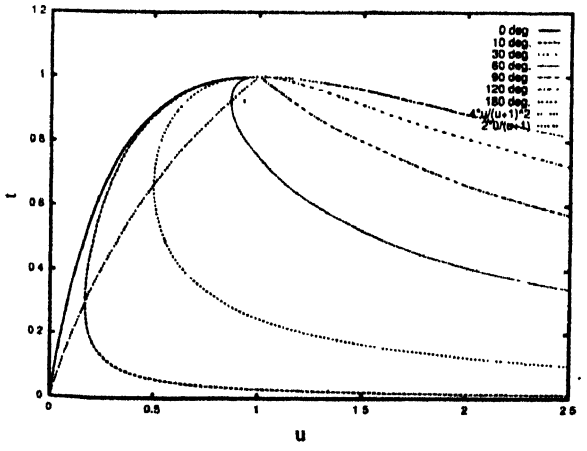

Figure 1. Kinematics of the electron excitation process using dimensionless variables t and u. The curves, starting from the left, represent $\theta = 0°$, 10°, 30°, 60°, 90°, 120° and 180°, respectively. Note that the curve connecting the maxima is the envelope curve [13] and the $\theta = 0°$ curve, the only fixed angle curve, connects continuously threshold, $t = 1$ and $t = 0$ and has its maximum at $t = 0$. All other curves for which $\theta \neq 0°$ avoid the limit point $t = 0$ and $u = 0$.

The dependence of t_2 on θ is weak at $\theta \sim 90°$. On the envelope curve [13] $t = 2u/(1+u)$ *i.e.* $K^2 = 2\omega\sin\theta(u = \sin\theta)$, we have $t_1 = t_2$. Figure 1 shows the variation of t with u for values of $\theta = 0-180°$. Also plotted is the envelope curve; it joins the maxima of the curves. Interestingly, the maximum of the $\theta = 0°$ curve is at $u = 0$. Clearly, the only curves that connect continuously $E = \omega$ and $E = \infty$ (the OOS limit) are the forward scattering and the envelope curves. However, the forward scattering curve is the only fixed angle curve that connects continuously the two energy limits. We note that $u \le 0.5$ for values of t up to about 0.9, implying that u is a natural expansion variable even at fairly low electron impact energies. This explains why sometimes first Born approximation is applicable even when E appears to be fairly low.

Eqs. (9) and (10) have been used to obtain the FSF [13]

$$\Phi(u) = f^0\left[1 - \frac{u}{u_{\max}}\right]e^{-(u/u_{\max})^2}, \tag{12}$$

where $u_{\max} = 0.25$ and f^0 is the OOS. Eq. (12) describes the locus of the AGOS points at various E values, with $E_{\min} \approx 2.5\ \omega$, such that $t = \frac{4u}{(1+u)^2}$. For any optically allowed transition, $\Phi(u)$ can be obtained from that of the H $1s$–$2p$ transition (or any other accurately known transition) and the corresponding OOS's. The FSF and the MOM have been used together to normalize measured relative electron DCS's [18–21] and to identify spurious behavior in both measured and calculated DCS's at and near $\theta = 0°$ [22,23]. Recently, the FSF has been generalized [24] for use in the nomalization of the relative experimental excitation or ionization DCS's or DDCS's. The new normalization [24] is effected beyond the FBA and without e:xtrapolation through the nonphysical region.

2.3. Generalized Lassettre expansion (GLE) :

At low electron impact energy, only a few partial waves are necessary to represent correctly a scattering process. When increasing the energy, more and more waves are contributing to the general process, and the partial wave expansion converges slower and slower. In particular, the presence of a square root singularity at $K^2 = 0$, prevents the partial wave expansion from converging there. Regge [25] has proposed to use complex angular momenta to produce a representation that converges for nonphysical transfer momenta. In this representation the amplitude is expanded into generalized partial waves. A full discussion on the application of the complex angular momentum to scattering problems is found in Connor [26]. Recently, a general method of calculating Regge poles for both singular and regular potentials has been developed and illustrated [27,28].

In the present case, where we analyze a K^2 region before the first minimum we can neglect the imaginary part of the

leading Regge pole (that controls the oscillations in the DCS) and write the generalized Lassettre expansion (GLE) (with only one moving Regge pole) [14]

$$f(E,K^2)=\frac{\mathrm{OOS}}{(1+x^2)^6}+A\frac{\omega}{E}\frac{}{(1+x^2)^{\nu(E)}}, \qquad (13)$$

where the OOS, f^0 and A do not depend on energy and where

$$\nu(E)=6+\frac{C}{\frac{E}{\omega}\ln\frac{E}{\omega}} \qquad (14)$$

The constant C can be computed directly from the Schrödinger equation through the general expressions given in Refs. [27,28] with the appropriate potentials used. Eqs. (13) and (14) give a global analysis of the AGOS in tenns of only three energy independent parameters A, C and f^0 (usually a known quantity determined independently).

The beauty of eq. (13) is structural simplicity; it manifests directly the energy dependence of the AGOS through the second term. We refer to this second term as the "moving Regge pole" contribution to the AGOS. The whole expression is referred to as the generalized Lassettre expansion [14] for obvious reasons. The GLE represented by eq. (13) differs from others [8,10] through the presence of the second term which also contains the square root singularity at $K = 0$, whose importance has been pointed out [29]. The GLE has been used to extract the OOS within 1% accuracy for the H $1s$–$2p$ transition from the accurate DCS's of Bray *et al* [30] when the data at 19.58 eV $\leq E \leq$ 200 eV were used.

3. Results

3.1. *General properties of the apparent generalized oscillator strength :*

In an appropriate representation, the physics simplifies considerably. Figure 1 depicts the kinematics of the electron excitation process using the dimensionless variables t and u for values of $\theta = 0$–$180°$. The curves, starting from the left, represent $\theta = 0°$, 10°, 30°, 60°, 90°, 120° and 180°, respectively. Note that the curve connecting the maxima is the envelope curve [13], and the $\theta = 0$ curve, the only fixed angle curve, continuously connects threshold, $t = 1$ and $t = 0$ and has its maximum at $t = 0$. All other curves for which $\theta \neq 0°$ avoid the limit point $t = 0$ and $u = 0$, corresponding to the optical oscillator strength. For values of t up to about 0.9, $u \leq 0.5$ implying that u is a natural expansion variable even at fairly low electron impact energies. Clearly, the Lassettre limit of the GOS ($t = u = 0$) can be reached only by staying on the $\theta = 0°$ curve, when starting from any E value.

The kinematic representation of Figure 1 permits the demonstration of the general properties of the AGOS [31].

We use the Li $2s$–$2p$ transition to elucidate small-angle electron scattering because of the availability of measurements [32, 33] and theoretical calculations [34, 35] over a wide range of electron impact energies and scattering angles. These data provide a stringent test of our approach and *vice versa*. Figure 2 shows the AGOS *versus* t from the data of Bray *et al* [35] at $\theta = 0°$, 1°, 3°, 5°, 10° and 15°, starting with the top curve at $\theta = 0°$, down to the bottom curve at $\theta = 15°$, as t varies from $t = 0.00185$ ($E = 1000$ eV) to $t = 0.185$ ($E = 10$ eV). The Bray *et al* [35] data demonstrates excellently how the AGOS's should approach the OOS limit as $t \to 0$ ($E \to \infty$) and θ decreases from 15° down to 0°. This behavior is general and is useful for identifying spuriously behaved data [31]. Also included in Figure 2 at $\theta = 3°$, 5° and 10° (crosses, dashed crosses and pluses, respectively) are the

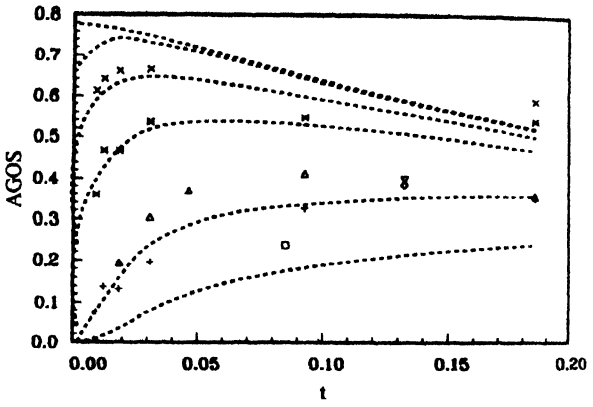

Figure 2. Apparent generalized oscillator strength AGOS *versus* t for the transition Li $2s$–$2p$ The data of Bray *et al* [35] at $\theta = 0°$, 1°, 3°, 5°, 10° and 15° are represented by the dashed curves, from top ($\theta = 0°$) to bottom ($\theta = 15°$), while the calculation of Madison *et al* [34] is shown only at $\theta = 10°$ (triangles) .The measurements of Vuskovic *et al* [32] are shown at $\theta = 3°$ (crosses), $\theta = 5°$ (dashed crosses) and at $\theta = 10°$ (pluses); those of Karaganov *et al* [33] are shown at $\theta = 0°$ (diamond), $\theta = 10°$ (inverted triangle) and at $\theta = 12°$ (square).

measured data points of Vuskovic *et al* [32]. The agreement with the data of Bray *et al* [35] is excellent, except at $t = 0.185$ ($E = 10$ eV), where the measured data are above the zero curve for both $\theta = 3°$ and 5°. We note that at 10 eV the AGOS's at $\theta = 0°$, 3° and 5° are close together; nevertheless they are still within the experimental errors. Furthermore, it becomes difficult to distinguish between, for example the AGOS's belonging to $\theta = 0°$ and 5° for $t \to 1$ and $E \to \infty$ Also shown in the figure are the calculated values of Madison *et al* [34] at $\theta = 0°$, represented by the triangles and the Karaganov *et al* [33] data at $\theta = 0°$ (diamond), $\theta = 10°$ (inverted triangle) and $\theta = 12°$ (square). For this measurement, the zero degree data point appears inaccurate.

Since experiments tend to experience problems in measuring reliably the DCS's at and near $\theta = 0°$, the variation of the AGOS with t for Li $2s$–$2p$ can be used to investigate

the behavior of the data of Vuskovic *et al* [32], Karaganov *et al* [33] and Madison *et al* [34] at $\theta = 0$. In Figure 3 is contrasted the data from the DCS measurements [32,33] and

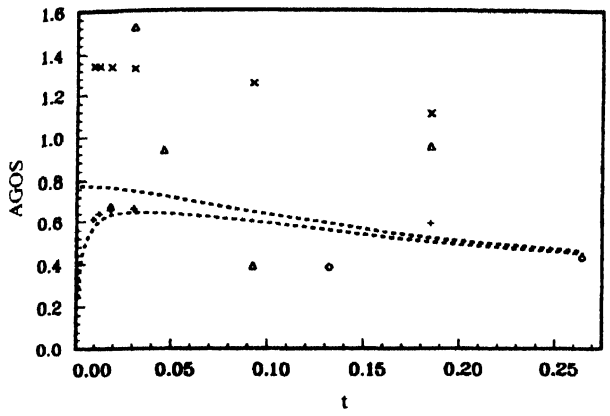

Figure 3. Comparison of the apparent generalized oscillator strength AGOS *versus* t for Li $2s$–$2p$ from the DCS measurements of Vuskovic *et al* [32] and Karaganov *et al* [33] with the Madison *et al* [34] calculation as well as the CCC calculation of Bray *et al* [35] at $\theta = 0°$ for values of E ranging from 7 eV to 1000 eV. The dashed curves are from Ref. [35] at $\theta = 0°$ (top curve) and $\theta = 3°$ (bottom curve). Note that the Vuskovic *et al* measurement at $\theta = 0°$ (crosses) simply requires normalization and at $\theta = 3°$ (pluses) agrees very well with the calculation of Ref. [35].

the theoretical calculations [34,35] at $\theta = 0°$ for values of E varying from 7 to 1000 eV. Also included for comparison are the Bray *et al* [35] and Vuskovic *et al* [30] data at $\theta = 3°$. As already seen in Figure 2, the Bray *et al* [35] data represent the zero scattering excellently. We therefore conclude that the Madison *et al* [34] data behave spuriously, but only at zero scattering angles. The measurement of Karaganov *et al* at 14 eV (diamonds) underestimates the zero degree data of Bray *et al* [35], while at 7 eV it agrees excellently with them. We note that near 1000 eV the $\theta = 0°$ and $\theta = 3°$ data are well separated, while those near $E = 7$ eV are almost indistinguishable. Contrary to common belief, it is easier to separate in angle measured data at high E than at low E.

3.2 *The Lassettre limit theorem :*

In this section we demonstrate the applicability of the Lassettre limit theorem, *viz.* $\lim_{K^2 \to 0} f(E, K^2) = f^0$, regardless of the electron impact energy. In Figure 1 we demonstrated that the $\theta = 0°$ curve is the only fixed scattering angle trajectory that connects continuously $E = \omega (t = 1)$ and $E = \infty (t = 0)$, the OOS limit, without involving the nonphysical region. No other trajectories at a fixed angle can lead to the OOS limit, although all begin at $t = 1$. For example, the 10° curve clearly avoids the OOS limit as $E \to \infty$. We note that although the second curve, called the envelope curve [13], also connects $E = \omega$ and $E = \infty$ continuously, but it does so not at a fixed angle. Furthermore, we saw that as $E \to \omega$, the angular dependence of eq. (10) is eliminated; all the small angular curves merge with the $\theta = 0°$ curve as $E \to \omega$. Therefore, the small angle, approximately $\theta \leq 15°$ (the angular regime of interest of this paper), behavior can be approximated by that of the $\theta = 0°$ curve as $E \to \omega$.

In Figure 4 we show the AGOS *versus* E for the H $1s$–$2p$ transition at $\theta = 0°$, 5° and 10°. The solid curves are calculated

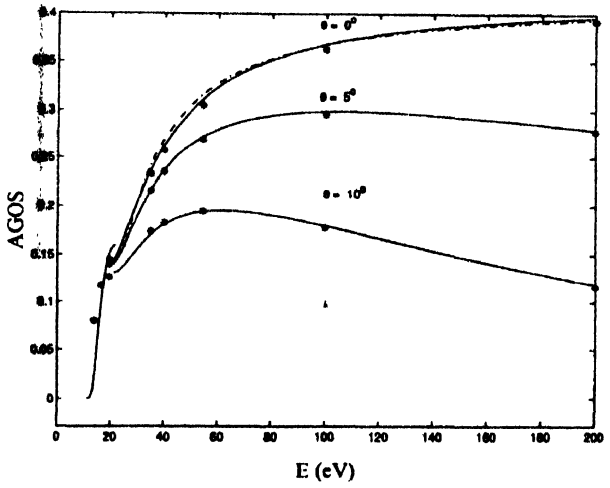

Figure 4. Comparison of the apparent generalized oscillator strength G for H $1s$–$2p$ as a function of E from the data of Bray, Konovalov and McCarthy [30] (**) and the GLE (–) at $\theta = 0°$, 5° and 10°. Near $E = \omega$ ($E \leq 20$ eVi, approximately) the data corresponding to $\theta = 0°$, 5° and 10° become indistinguishable as required by the kinematics of Figure 1. Also included is the FSF (– · –).

using the values of the constants A and C obtained by Felfli *et al* [14]. The dash-dot curve is the forward scattering function of Avdonina *et al* [13], while the asterisks represent data from Bray *et al* [30]. The agreement between the Bray *et al* [30] data and the GLE is excellent down to near threshold. Note that the 10° and 5° curves merge with the zero degree curves as $E \to \omega$, consistent with the Kinematics, Figure 1. As $E \to 200$ eV, the separation among the various curves becomes larger in comparison with that near $E \to \omega$. That the AGOS curves other than that corresponding to $\theta = 0°$ must vanish as $E \to \infty$, follows from eq. (13). As $E \to \infty$, the second term becomes negligible and only the Born term survives, *viz.*

$$f(E, K^2) = \frac{f^0}{(1+x^2)^6} - \frac{f^0}{[1+4DE(1-\cos\theta)]^6}, \tag{15}$$

where D is a constant independent of E. When $\theta = 0°$ in eq. (15), $f(E, K^2) = f^0$. Therefore, the $\theta = 0°$ trajectory of the AGOS is the only fixed scattering angle curve for reaching the Lassettre limit when starting from any E-value and without involving the nonphysical region. This demonstrates clearly the single-pole dominance of the scattering process at forward scattering. For any non-zero scattering angle, $f(E, K^2) \sim \left(\frac{\omega}{E}\right)^6$ which approaches zero as $E \to \infty$. Consequently, the $\theta = 5°$

and 10° (or any $\theta \neq 0°$) AGOS curves actually go to zero as $E \rightarrow \infty$, leaving only the forward scattering curve to satisfy the Lassettre limit theorem, consistent with the Kinematics of Figure 1. Thus establishing the applicability of the Lasettre limit theorem regardless of the electron impact energy required an appropriate universal representation of the Kinematics and the AGOS.

Some immediate consequences of the Lassettre limit theorem are worth mentioning. From Figure 4 it is now clear that knowing the absolute values of the DCS's at $\theta = 0°$ as a function of E, the data can be used to determine the value of the OOS [9]; the accuracy being determined by that of the DCS's. This, a superior approach because it avoids completely the extrapolation of the AGOS, particularly through the nonphysical region, should be contrasted with that used in Ref. [9]. Experimentally, it would be easier to separate the angular dependence of the AGOS's as $E \rightarrow \infty$, rather than those near threshold. Most importantly, the GLE at $\theta = 0°$ defines the long-sought-after unique normalization curve of the AGOS's to the OOS. This implies that for absolute data, the AGOS at any impact energy must lie on this curve; otherwise the data point at the given impact energy must be shifted up or down so that it is on the curve. Interestingly, it would be difficult to separate in general spuriously behaved data points from improperly normalized data points. However, the self-consistency of the data as a function of angle or K^2 can be ascertained using the MDM as was demonstrated by Felfli and Msezane [18] and Marinkovic *et al* [19].

3.3. *Normalization of differential cross sections :*

Since at $\theta = 0°$ the GLE connects continuously the $E = \omega$ and $E = \infty$ (the OOS) limits, it therefore represents the long-sought-after normalization curve to the OOS, regardless of the impact energy and without involving the nonphysical region. In this section we extract the normalization curves appropriate to the optically allowed transitions in H, He and Xe to demonstrate correctly normalized data and/or spuriously behaved data at or near $\theta = 0°$. To analyze these transitions using the GLE we need the values of A and C in eq. (13) of the GLE. As pointed out by Felfli *et al* [14], C can be determined directly by solving the Schrödinger equation, a laborious process, or from the measured data. However, for the present purpose A and C will be extracted in a simple way. At $\theta = 0°$ the GLE and FSF, including its generalized version [24], are matched at two arbitrary impact energies, one high, E_2 and the other low, E_1. Table 1 shows the results of such a determination. The constants are not too sensitive to the choice of E_1 and E_2 as long as they are reasonably separated. We note that, while the FSF can be used only at $\theta = 0°$, the GLE can also be employed for $\theta \neq 0°$ as shown in Figure 4. The curves at $\theta = 0°$, 5°, 10° were obtained using the same constants from Felfli *et al* [14], given in Table 1. Also, the GLE can be used to determine OOS's [14] from measured absolute DCS's.

Table 1. GLE constants for the systems of interest. f^0 values are from Felfli *et al* [14].

System	A	C	E_1(eV)	E_2(eV)	f^0
H $1s$–$2p$	−3.340	14.565	25.5	152.0	0.415
	−2.980[a]	12.200[a]			
He 1^1S–2^1P^0	- 1.217	0.370	24.0	84.0	0.278
Xe[3/2]	−1.827	5.262	17.0	64.0	0.230

Unlike for the H $1s$–$2p$ transition, there are many measurements and calculations of the DCS's for the He $1\,^1S$–$2\,^1P^0$ transition at and near $\theta = 0°$, the angular region of our interest. Since in this paper we want to demonstrate the applicability of the GLE, we have selected the measurements [36–39] and calculations [39–41]. Combined, they cover the electron impact energy range $23.2 \leq E \leq 1500$ eV and the angular regime $0° \leq \theta \leq 180°$. Because of the availability of the measured data at and near $\theta = 0°$, the four measurements are suitable for demonstrating the normalization capability of the GLE. Define the energy $Z = E/\omega$.

In Figure 5 various selected calculations [39–41] and measurements [36–39] of the AGOS's at $\theta = 0°$, for He

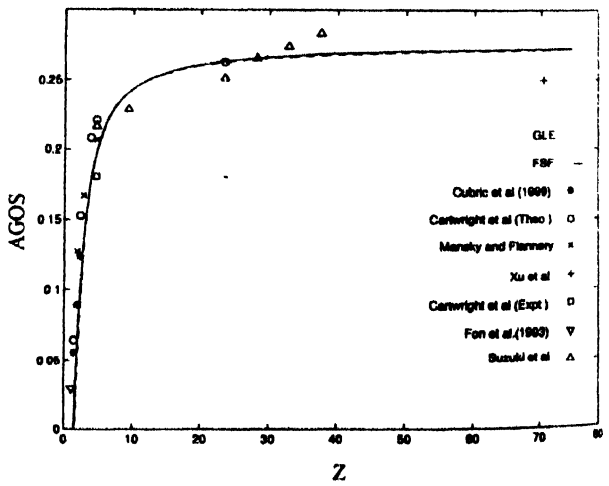

Figure 5. The apparent generalized oscillator strength G for He $1\,^1S$–$2\,^1P^0$ from the GLE (–) and FSF (- - -) are compared to those from various measurements [36–39] and calculations [39–41]. The variable $Z = E/\omega$ is used for the horizontal axis.

$1\,^1S$–$2\,^1P^0$ are compared with the OLE and FSF curves for $23.2 \leq E \leq 1500$ eV. The results demonstrate that the GLE can be employed to normalize relative measurements to the OOS at any E and/or assess the reliability of measured or calculated electron DCS's at $\theta = 0°$, even very close to threshold. We obtained the AGOS's at $\theta = 0°$ for $E = 100$ eV and 1500 eV for the measured data [37,38] using the MDM

because the last measurements were at 1.2° and 2°, respectively. Although the data point of Xu *et al* appears significantly lower than the FSF and GLE curves, it is, nevertheless within the experimental errors. Also, the measurement [37] appears to be increasing away from the OOS limit as E increases from 600 eV to 800 eV. This behavior is incorrect, but is still within the experimental errors. Just like for the H $1s-2p$ transition, the GLE represents very well the measured He $1^1S-2\,^1P^0$ data over a wide range of E-values.

Suzuki *et al* [42] have measured the electron excitation DCS's for the Xe [3/2, 1/2] $6s$ states from ground state at 100, 400 and 500 eV, down to scattering angles $\theta_s = 2.45°$, 1.4° and 1.5°, respectively. Ester and Kessler [9] have measured absolute DCS's for the same transitions at E-values between 15 and 100 eV, but only down to $\theta_s = 6°$. Both experiments also determined OOS's. Ester and Kessler also demonstrated that their data at 100 and 80 eV were compatible with Lassettre's limit theorem, while those for $E \leq 40$ eV were not. To apply the GLE to both measurements, we must first obtain data at $\theta = 0°$ from the respective data sets using the MDM. Within the experimental errors, the data points at $\theta = 0°$ must lie on the corresponding GLE curve as in Figure 4. Figure 6 compares the Suzuki *et al* [42] data with that of Ester and Kessler for the Xe [3/2] $6s$ state. The GLE and FSF curves are also included, and are in good agreement

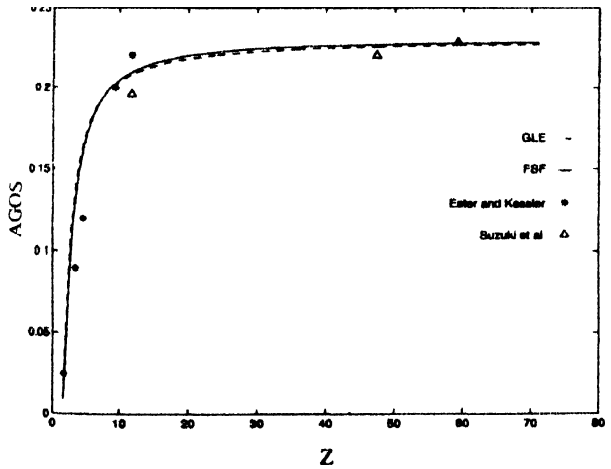

Figure 6. Comparison of the apparent generalized oscillator strength G as a function of Z for the excitation of the Xe [3/2]$6s$ state from the GLE (–) and the FSF (---) with data from the measurements of Suzuki *et al* [42] and Ester and Kessler [9].

with the measurements within their errors. We note that Khakoo *et al* [1] also measured the DCS's for the features 1 and 2 of Xe for $0° \leq \theta \leq 180°$ at 15, 20 and 30 eV. However, their data for feature 2 are ill-behaved near at 15 and 20 eV; the rest of their data behave excellently.

4. Conclusion

In this paper we have demonstrated, in an appropriate representation, the general properties of the AGOS, thus providing a stringent test of small angle electron scattering measurements and calculations. The recent generalized Lassettre expansion, employing a single moving Regge pole, has been used to establish the applicability of the Lassettre limit theorem, regardless of the electron impact energy and without the involvement of the nonphysical region of the AGOS. Furthermore, at forward scattering the GLE provides the long-sought-after normalization curve to the OOS of the measured relative electron DCS's through the AGOS. Illustrative examples for optically allowed transitions come from H, He, Li and Xe; others can be found in Felfli *et al* [44], including for a molecular transition. The work presented here represents a component of a more extensive international collaboration investigating correlation effects in atomic transitions, Deb *et al* [45], photoionization processes, Haque *et al* [46] and Gorczyca *et al* [47] as well as in generalized oscillator strengths of dipole, monopole and quadrupole transitions, Amusia *et al* [48].

Acknowledgments

Work was supported by DoE, Division of Chemical Sciences, Office of Basic Energy Sciences, Office of Energy Research (AZM), NASA-PACE and NSF.

References

[1] M A Khakoo, M Larsen, B Paolini, X Guo, I Bray, A Stelbovics, I Kanic and S Trajmar *Phys. Rev Lett* **82** 3980 (1999), M A Khakoo, M Larsen, B Paolini, X Guo, I Bray, A Stelbovics, I Kanic, S Trajmar and G K James *Phys Rev.* **A61** 012701 (2000)

[2] V Karaganov, I Bray and P J O Teubner *Phys. Rev* **A59** 4407 (1999)

[3] I D Williams, A Chutjian and R J Mawhorter *J. Phys.* **B19** 2189 (1986)

[4] K Xu, Z Zhong, S Wu, R Feng, S Ohtani, T Takayanagi and A Kimota *Science in China (Series A)* **38** 368 (1995)

[5] H A Bethe *Ann. Phys* **5** 325 (1930)

[6] W F Miller and R L Platzman *Proc R. Soc London Ser* **A70** 299 (1957)

[7] E N Lassettre, A Skerbele and M A Dillon *J. Chem. Phys* **50** 1829 (1969)

[8] K N Klump and E N Lassettre *J. Chem Phys* **68** 886 (1978); M Ismail and P J O Teubner *J. Phys* **B28** 4149 (1995)

[9] T Ester and J Kessler *J. Phys.* **B27** 4295 (1994)

[10] A Haffad, Z Felfli, A Z Msezane and D Bessis *Phys. Rev. Lett.* **76** 2456 (1996)

[11] M Ismail and P J O Teubner *J. Phys.* **B28** 4149 (1995)

[12] Zhifan Chen and A Z Msezane *J. Chem. Phys.* **102** 3888 (1995)

[13] N Avdonina, Z Felfli and A Z Msezane *J. Phys* **B30** 2591 (1997)

[14] Z Felfli, A Z Msezane and D Bessis *Phys. Rev. Lett.* **81** 963 (1998)

[15] M Inokuti *Rev. Mod Phys.* **43** 297 (1971)

[16] Zhifan Chen and A Z Msezane *Phys. Rev.* **A55** 812 (1997)

[17] P Ozimba and A Z Msezane *Chem. Phys.* **246** (1999)

[18] Z Felfli and A Z Msezane *J. Phys.* **B31** L165 (1998)

[19] B Marinkovic, Z D Pejcev, R Panajotovic, D M Filipovic, Z Felfli and A Z Msezane *J. Phys* **B32** 1949 (1999)

[20] B Marinkovic, C Z Szmytkovwski, V Pejsev, D Filipovic and L Vuskovic *J. Phys.* **B19** 2365 (1986)

[21] S Wang, S Trajmar and P W Zetner *J. Phys.* **B27** 1613 (1994)

[22] A Z Msezane, Z Felfli and Z Chen *J Phys.* **B29** L817 (1996)

[23] A Z Msezane and D Bessis *J. Phys.* **B30** 445 (1997)

[24] N Avdonina, Z Felfli and A Z Msezane *J. Phys.* **B32** 5179 (1999)

[25] V De Alfaro and T Regge *Potential Scattering* (North-Holland, Amsterdam) (1965)

[26] J N L Connor *J. Chem. Soc. Faraday Trans.* **86** 1627 (1990)

[27] D Vrinceanu, A Z Msezane and D Bessis *Chem Phys. Lett.* **311** 395 (1999)

[28] D Vrinceanu, A Z Msezane and D Bessis *Phys. Rev* **A62** 022719 (2000)

[29] W M Huo *J Chem. Phys.* **60** 3544 (1974)

[30] I Bray, D A Konovalov and I E McCarthy *Phys. Rev.* **A44** 5586 (1991)

[31] N B Avdonina, Z Felfli, D Fursa and A Z Msezane *Phys. Rev.* **A62** 014703 (2000)

[32] L Vuskovic, S Trajmar and D F Register *J. Phys.* **B15** 2517 (1982)

[33] V Karaganov, I Bray and P J O Teubner *Phys. Rev.* **A59** 4407 (1999)

[34] D H Madison, R P McEachran and M Lehmann *J. Phys. B bf* 27 1807 (1994)

[35] I Bray, D V Fursa and I E McCarthy *Phys. Rev.* **A47** 1101 (1993)

[36] D Cubric, D J L Mercer, J M Channing, G C King and F H Read *J. Phys.* **832** L45 (1999)

[37] T Y Suzuki, H Suzuki, F J Currell, S Ohtani, Y Sakai, T Takayanagi and K Wakiya *Phys. Rev.* **A57** 1832 (1998)

[38] K Z Xu, R F Fegbn, S L Wu, Q Ji, X J Zhang, Z P Zhong and Y Zheng *Phys. Rev.* **A53** 3081 (1996)

[39] D C Cartwright, G Csanak, S Trajmar and D F Register *Phys Rev* **A45** 1602 (1992)

[40] E J Mansky and M R Flannery *J. Phys.* **823** 4573 (1990)

[41] W C Fon, K P Lim and P M J Sawey *J. Phys* **B26** 4201 (1993)

[42] T Y Suzuki, Y Sakai, B S Mill, T Takayanagi, K Wakiya, H Suzuki T Inaba and H Takuma *Phys Rev.* **A43** 5867 (1991)

[43] M A Khakoo, S Trajmar, L R LeClair, I Kanik, G Csanak and C J Fontes *J Phys* **B29** 3455 (1996)

[44] Z Felfli, N Embaye, P Ozimba and A Z Msezane *Phys Rev* A63 012709 (2001)

[45] N C Deb, G P Gupta and A Z Msezane *Phys Rev* **A60** 2569 (1999)

[46] N Haque, H S Chakraborty, P C Deshmukh, S T Manson A Z Msezane, N C Deb, Z Felfli and T W Gorczyca *Phys Rev* **A60** 4577 (1999)

[47] T W Gorczyca, Z Felfli, N C Deb and A Z Msezane *Phys Rev* **A63** 010702 (R) (2001)

[48] M Ya Amusia, L V Chernysheva, Z Felfli and A Z Msezane *Phys Rev.* A submitted (2001)